

## *s*-PROCESS IMPLICATIONS FROM OSMIUM ISOTOPE ANOMALIES IN CHONDRITES

MUNIR HUMAYUN

National High Magnetic Field Laboratory and Department of Geological Sciences, Florida State University,  
1800 East Paul Dirac Drive, Tallahassee, FL 32310; humayun@magnet.fsu.edu

AND

ALAN D. BRANDON

NASA Johnson Space Center, Mail Stop KR, Houston, TX 77058; alan.d.brandon@nasa.gov

Received 2007 April 2; accepted 2007 June 5; published 2007 July 3

### ABSTRACT

Correlated isotopic anomalies in osmium ( $^{186}\text{Os}$ ,  $^{188}\text{Os}$ ,  $^{190}\text{Os}$ , measured with respect to  $^{189}\text{Os}$ ) extracted from primitive carbonaceous chondrites tightly constrain the  $\sigma_n(^{190}\text{Os})/\sigma_n(^{188}\text{Os})$  ratio to be  $0.859 \pm 0.042$  ( $\pm 5\%$ ). A recent measurement of the Maxwellian-averaged neutron-capture cross sections (MACSs) for  $^{186, 187, 188}\text{Os}$  lowered the  $\sigma_n(^{188}\text{Os})$  by 27% but did not measure  $\sigma_n(^{190}\text{Os})$ . From the  $\sigma_n(^{190}\text{Os})/\sigma_n(^{188}\text{Os})$  ratio, we infer  $\sigma_n(^{190}\text{Os}) = 249 \pm 18$  mbarns for internal consistency with the new MACSs for the other Os isotopes. This approach is applicable to other isotopic anomalies in *r*-process/*s*-process ratios derived from meteorites for nuclei that do not have branching points between them. Branching at  $^{185}\text{W}$  and  $^{186}\text{Re}$  makes the  $^{186}\text{Os}/^{188}\text{Os}$  ratio a neutron dosimeter for the *s*-process that, with the new cross sections, yields an average neutron density,  $n_n \sim 3 \times 10^8 \text{ cm}^{-3}$ . This low neutron density is consistent with previous results from Sr, Zr, Mo, and Ba isotopes that indicated a minor contribution from the  $^{22}\text{Ne}(\alpha, n)^{25}\text{Mg}$  neutron source relative to the  $^{13}\text{C}(\alpha, n)^{16}\text{O}$  neutron source.

*Subject headings:* nuclear reactions, nucleosynthesis, abundances — solar system: general

### 1. INTRODUCTION

Isotope anomalies in chondrites provide us with a wealth of information on stellar nucleosynthesis prior to solar system formation. New developments in mass spectrometry have made possible the measurement of anomalies in the ratio of slow neutron-capture process (*s*-process) to rapid neutron-capture process (*r*-process) isotopes for Mo (e.g., Yin et al. 2002), Ru (Papanastassiou et al. 2004), Ba (Ranen & Jacobsen 2006), and Os (Brandon et al. 2005). These anomalies were interpreted either in terms of an inhomogeneous distribution in the solar nebula (e.g., Yin et al. 2002) or in terms of the selective dissolution of presolar grains that carried large isotope anomalies (Brandon et al. 2005). New results confirm that primitive chondrites retain both excesses and deficiencies of *s*-process Os (Reisberg et al. 2007; Yokoyama et al. 2007) and that metamorphosed chondrites (Brandon et al. 2005) or alkaline fusions of primitive chondrites (Yokoyama et al. 2007) yield Os isotopically identical to that of the Earth. These results imply that acid-insoluble, presolar grains carry enough Os to influence the bulk isotopic composition of Os in chondrites, the recovery and individual analysis of which should reveal important clues to *s*-process nucleosynthesis in the W-Re-Os region. Currently, individual isotopic analyses of presolar grains for Sr, Zr, Mo, Ru, and Ba are available (e.g., Nicolussi et al. 1998; Lugaro et al. 2003).

Nucleosynthesis in the W-Re-Os region is of particular interest for *s*-process studies due to branching at  $^{185}\text{W}$  and  $^{186}\text{Re}$  (Fig. 1). Osmium has two *s*-only isotopes,  $^{186}\text{Os}$  and  $^{187}\text{Os}$  (shielded by  $^{186}\text{W}$  and  $^{187}\text{Re}$ , respectively), and the *s*-process contributes proportionally more to the abundances of the even isotopes,  $^{188}\text{Os}$  and  $^{190}\text{Os}$ , than it does to the odd-*A*  $^{189}\text{Os}$ , which is dominated by the *r*-process. Since there are no branch points between  $^{188}\text{Os}$  and  $^{190}\text{Os}$ , the ratio of the *s*-process contributions to these two isotopes is approximately equal to the inverse ratio of their neutron-capture cross sections ( $\sigma_n$ ). From Figure 1, it can be seen that the *s*-process flow can bypass the *s*-only  $^{186}\text{Os}$  isotope at both the  $^{185}\text{W}$  branching point and the  $^{186}\text{Re}$  branching

point, leading directly to the synthesis of  $^{188}\text{Os}$ . Such branching points provide us with important information on the temperature and neutron density of the *s*-process. Both branching points are relatively insensitive to temperature (Takahashi & Yokoi 1987) and are therefore good indicators of neutron density in the *s*-process (Käppeler et al. 1991; Brandon et al. 2005). Employing the  $\sigma_n$  values of Bao et al. (2000), Brandon et al. (2005) inferred neutron densities that were 2–4 times higher than canonical solar system values (Arlandini et al. 1999) from *s*-process anomalies in chondrites. Exploring the role of variable neutron density in the *s*-process depends heavily on accurate  $\sigma_n$  values for the osmium isotopes.

Recently, Mosconi et al. (2006) reported a new set of  $\sigma_n$  values for  $^{186, 187, 188}\text{Os}$  isotopes that significantly lowered  $\sigma_n(^{188}\text{Os})$  by 27% from the recommended value (Bao et al. 2000). Unfortunately, Mosconi et al. (2006) did not measure  $\sigma_n(^{190}\text{Os})$ , which is essential for the interpretation of Os isotope anomalies in chondrites or presolar grains. This Letter employs the geochemical measurements of Os isotope anomalies in chondrites to constrain the value of  $\sigma_n(^{190}\text{Os})$  and examines the impact of the new  $\sigma_n$  values for  $^{186, 188}\text{Os}$  (Mosconi et al. 2006) on neutron density in the stellar sites of the *s*-process.

#### 2.1. Geochemical Constraints on $\sigma_n(^{190}\text{Os})$

As noted above (Fig. 1), there are no branching points in the *s*-process path between  $^{188}\text{Os}$  and  $^{190}\text{Os}$ , so that isotope anomalies due to variations of the *s*-process/*r*-process contributions in chondrites provide us with direct information on the ratio of the cross sections of these nuclides. This information cannot be obtained from the solar system abundances of Os isotopes, formerly the only source of data for *s*-process studies, since the separate contributions of the *r*-process and *s*-process are not independently known. Following the convention of Brandon et al. (2005), Os isotope ratios have  $^{189}\text{Os}$  in the denominator and have been normalized to the solar system value of  $^{192}\text{Os}/^{189}\text{Os}$  (the two *r*-process-dominated isotopes) to correct for instrumental mass bias. Since the isotope anomalies are on

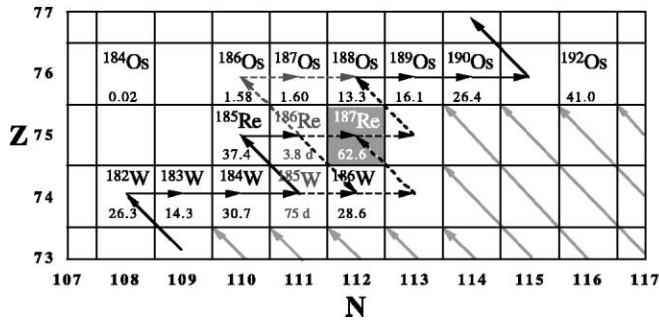


FIG. 1.—The  $s$ -process nucleosynthesis pathway in the W-Re-Os region. Stable nuclides with isotopic abundances are shown as black letters; long-lived radioactive nuclides are shown as white letters with gray background; and short-lived radioactive nuclides with half-lives are shown as gray letters. The  $r$ -process is shown as oblique gray arrows emerging from the lower right-hand corner of the field and terminating at the first stable nuclide. The  $s$ -process pathway (solid black arrows) comes through monoisotopic  $^{181}\text{Ta}$ , branches at  $^{185}\text{W}$ , and then again at  $^{186}\text{Re}$ . Both branches join at  $^{188}\text{Os}$  ( $s$ -process branches are depicted as dashed arrows). Three processes occur at  $^{186}\text{Re}$ :  $\beta^-$  decay to  $^{186}\text{Os}$  (97%), electron capture to  $^{186}\text{W}$  ( $\sim 3\%$ ), and neutron capture to  $^{187}\text{Re}$ .

the order  $10^{-4}$ , these anomalies are reported in the  $\epsilon$ -notation (Brandon et al. 2005):

$$\epsilon^x\text{Os} = \left[ \frac{(^x\text{Os}/^{189}\text{Os})_{\text{sample}}}{(^x\text{Os}/^{189}\text{Os})_{\text{ssa}}} - 1 \right] \times 10^4, \quad (1)$$

where  $x$  denotes the isotope mass and ssa denotes the solar system average Os isotope composition determined from equilibrated chondrites (Brandon et al. 2005). The slope of the correlation line ( $m$ ) in a plot of  $\epsilon^{190}\text{Os}$  versus  $\epsilon^{188}\text{Os}$  is

$$m = \frac{R_{\text{ssa}}^{188} \sigma_n(^{188}\text{Os})}{R_{\text{ssa}}^{190} \sigma_n(^{190}\text{Os})}, \quad (2)$$

where  $R_{\text{ssa}}$  is the isotope ratio (normalized to  $^{189}\text{Os}$ ) of the average solar system Os isotope composition.

Figure 2 shows chondritic Os isotope anomalies in  $\epsilon^{190}\text{Os}$  versus  $\epsilon^{188}\text{Os}$ . A least-squares fit to the chondrite data (Fig. 2) provided a slope of  $0.587 \pm 0.029$  ( $1\sigma$ ) (Table 1). Brandon et al. (2005) provided precise measurements of the Os isotope ratios of average ordinary chondrites from which we derive  $(^{188}\text{Os}/^{190}\text{Os})_{\text{ssa}} = 0.5040813 \pm 38$  ( $2\sigma$ ). Application of equation (2) yields the ratio of the  $\sigma_n$  values for  $^{190}\text{Os}$  and  $^{188}\text{Os}$  to be  $0.859 \pm 0.042$  ( $1\sigma$ ), without considering the effect of the stellar enhancement factors. Combining this with  $\sigma_n(^{188}\text{Os}) = 291 \pm 15$  mbarns at a reference thermal energy of 30 keV (Mosconi et al. 2006) yields  $\sigma_n(^{190}\text{Os}) = 249 \pm 18$  mbarns ( $\pm 7\%$ ). The stellar enhancement factor (SEF) for  $^{190}\text{Os}$  is 1.00 from 5 to 30 keV, while the SEF for  $^{188}\text{Os}$  is 1.00 from 5 to 20 keV but increases to 1.02 at 30 keV (Bao et al. 2000). Thus, the effect of the SEF would decrease our  $\sigma_n(^{190}\text{Os})$  by 2% at 30 keV. However, since the calculated  $\sigma_n$  is based on natural data, and since the thermal energy at the site of the  $s$ -process is estimated

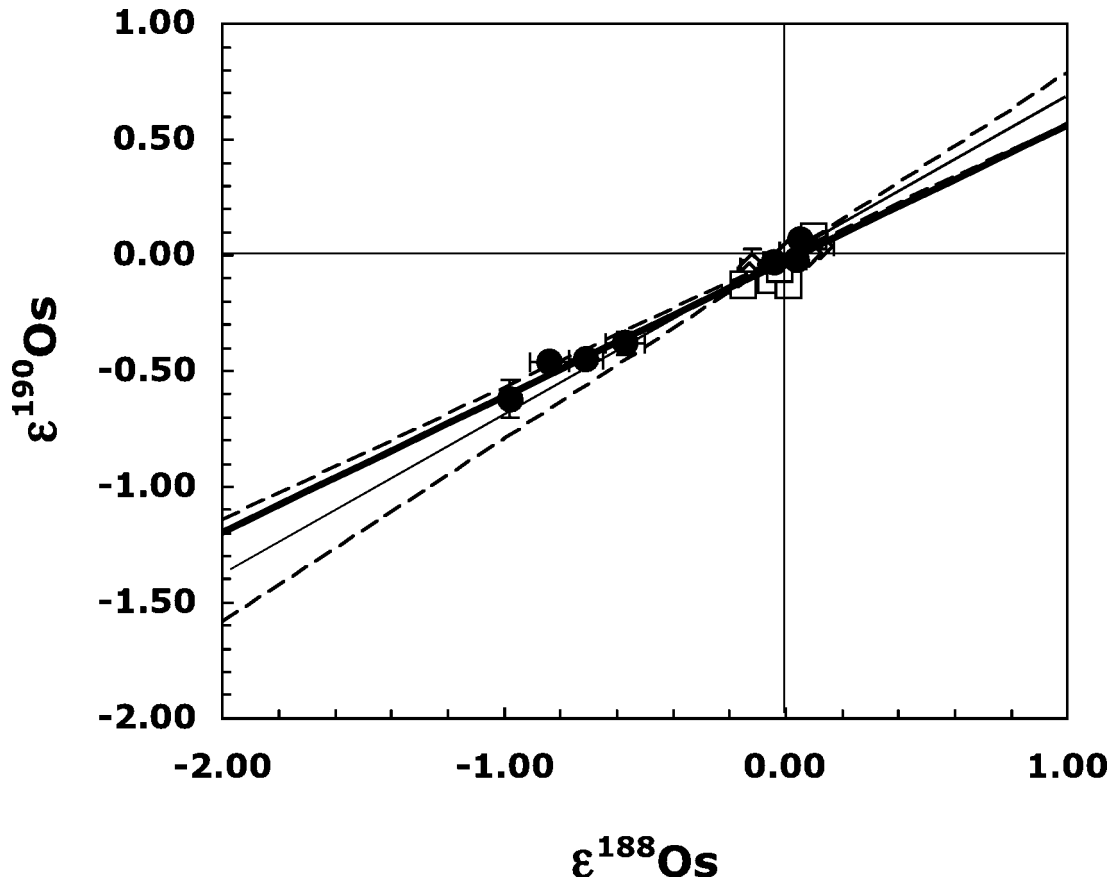


FIG. 2.—Chondritic Os isotope anomalies in  $\epsilon$ -values for the  $^{190}\text{Os}/^{189}\text{Os}$  and  $^{188}\text{Os}/^{189}\text{Os}$  ratios (see text for definition) for ordinary chondrites (open diamonds), enstatite chondrites (open squares), and carbonaceous chondrites (filled circles) from Brandon et al. (2005). The thick solid line is a least-squares fit to the chondrite data (slope =  $0.587 \pm 0.029$ ). The thin solid line represents the slope calculated from the cross sections of Bao et al. (2000), with  $1\sigma$  error limits (dashed lines), and is constrained to pass through the origin.

TABLE 1  
MACSs (30 keV) AVAILABLE FOR Os ISOTOPES (mbarns) AND THEIR PREDICTED SLOPES ON AN  $\epsilon^{190}\text{Os}$  VERSUS  $\epsilon^{188}\text{Os}$  PLOT

Source	$\sigma_n(^{188}\text{Os})$	$\sigma_n(^{190}\text{Os})$	$\sigma_n(^{190}\text{Os})/\sigma_n(^{188}\text{Os})$	Slope $\epsilon^{190}\text{Os}$
Allen et al. (1971) .....	275	230	0.84	0.60
Holmes et al. (1976) .....	474	577	1.22	0.41
Browne & Berman (1981) .....	$395 \pm 24$	$296 \pm 45$	$0.75 \pm 0.12$	0.68
Harris (1981) .....	262	213	0.81	0.62
Winters et al. (1980) .....	$401 \pm 15$	...	...	...
Rauscher & Thielmann (2000) .....	338	212	0.63	0.80
Bao et al. (2000) .....	$399 \pm 15$	$295 \pm 45$	$0.74 \pm 0.12$	$0.68 \pm 0.11$
Mosconi et al. (2006) .....	$290 \pm 15$	...	...	...
This study (30 keV) .....	290	$249 \pm 18$	$0.859 \pm 0.042$	$0.587 \pm 0.029$
This study (23 keV) .....	$315 \pm 15$	$271 \pm 18$	...	...
This study (8 keV) .....	$527 \pm 22$	$453 \pm 29$	...	...

NOTE.—Calculated  $\sigma_n(^{190}\text{Os})$  at thermal energies of 8, 23 and 30 keV from this study.

to be 8 keV with a marginal contribution at 23 keV (e.g., Lugaro et al. 2003), the effect of SEF is not included in Table 1.

Table 1 summarizes all the available experimental or theoretical  $\sigma_n$  ratios at 30 keV. The resulting slopes of the correlations in  $\epsilon^{190}\text{Os}$  versus  $\epsilon^{188}\text{Os}$  plots were calculated using equation (2). The  $\sigma_n(^{190}\text{Os})/\sigma_n(^{188}\text{Os})$  ratio is consistent for nearly all reported values (0.74–0.84), excluding that of Holmes et al. (1976), with the ratio derived by inversion of the chondrite data ( $0.859 \pm 0.042$ ). The recommended values of Bao et al. (2000) reproduce the observed slope within uncertainties (Fig. 2); however, Mosconi et al. (2006) give a  $\sigma_n(^{188}\text{Os})$  value that is 27% lower than that of Bao et al. (2000). Thus, we predict that new measurements for  $\sigma_n(^{190}\text{Os})$  should yield a value 20% lower than given by Bao et al. (2000) at 30 keV. Table 1 also lists  $\sigma_n(^{190}\text{Os})$  values for *s*-process thermal energies of 8 and 23 keV.

Unlike laboratory  $\sigma_n$  determinations, the  $\sigma_n(^{190}\text{Os})/\sigma_n(^{188}\text{Os})$  ratio obtained from geochemical measurements is directly applicable to thermal energies at *s*-process sites. The recommended  $\sigma_n$  values decrease by  $1/v$  for both  $^{188}\text{Os}$  and  $^{190}\text{Os}$  (Bao et al. 2000). However, the new  $\sigma_n(^{188}\text{Os})$  values do not show a simple  $1/v$  decrease in the energy range 5–30 keV (Mosconi et al. 2006). Thus, extrapolation of the  $\sigma_n(^{190}\text{Os})$  values obtained

here from geochemical measurements beyond the energy range applicable at the *s*-process sites should be viewed with caution. This is pertinent to stellar models of *s*-process nucleosynthesis (e.g., Arlandini et al. 1999), which may require new laboratory measurements of the MACSs for isotopes in the W-Re-Os region over a large range of thermal energies to enable better interpretations of the Os isotope data that have become available (Brandon et al. 2005; Reisberg et al. 2007; Yokoyama et al. 2007).

## 2.2. Neutron Density in the W-Re-Os Region

Brandon et al. (2005) noted that the slope of the canonical solar system *s*-process calculated from both the classical *s*-process analysis and a stellar model (Arlandini et al. 1999) on an  $\epsilon^{186}\text{Os}$  versus  $\epsilon^{188}\text{Os}$  plot is too steep to explain their chondrite Os isotope anomalies. They reconciled their data with the solar system *s*-process by proposing that an insoluble *s*-process component existed that had experienced an average neutron density that was 2–4 times higher than that of the average *s*-process in the solar system. We have reassessed the neutron density from the *s*-process branching at  $^{185}\text{W}$  and  $^{186}\text{Re}$  from its impact on the  $^{186}\text{Os}/^{188}\text{Os}$  *s*-process ratio by applying the classical model (Käppeler et al. 1991), with new  $\sigma_n(^{185}\text{W})$  and  $\sigma_n(^{186}\text{Re})$  values (Sonnabend et al. 2003) and new  $\sigma_n(^{186, 187, 188}\text{Os})$  values (Mosconi et al. 2006). The  $^{186}\text{Os}/^{188}\text{Os}$  ratio is shown as a function of neutron density in Figure 3 for the recommended  $\sigma_n$  values (Bao et al. 2000) and the new  $\sigma_n$  values (Mosconi et al. 2006). The  $^{186}\text{Os}/^{188}\text{Os}$  ratio at a given neutron density calculated with the new  $\sigma_n$  values is systematically 35% lower than with the previous values. The neutron density calculated from the classical *s*-process approach (Käppeler et al. 1991; Sonnabend et al. 2003) is shown, together with the  $^{186}\text{Os}/^{188}\text{Os}$  ratio calculated from their *s*-process abundances. The new neutron density calculated from the *s*-process  $^{186}\text{Os}/^{188}\text{Os}$  (0.545) endmember obtained from the chondrite Os isotope anomalies and the curve obtained using the new  $\sigma_n$  values (Mosconi et al. 2006) yields an average neutron density of  $\sim 3 \times 10^8 \text{ cm}^{-3}$  for *s*-process Os.

Arlandini et al. (1999) compared the *s*-process yields from the classical approach with those from a stellar model and found that neutron densities calculated by a stellar model more accurately reproduced the *s*-process abundances around branching points. They argued that the classical approach, with its assumption of an exponential distribution of neutron exposures, was inadequate for describing the neutron exposure of the *s*-process. The  $^{186}\text{Os}/^{188}\text{Os}$  yields obtained by Arlandini et al. (1999) for their stellar model and from application of the clas-

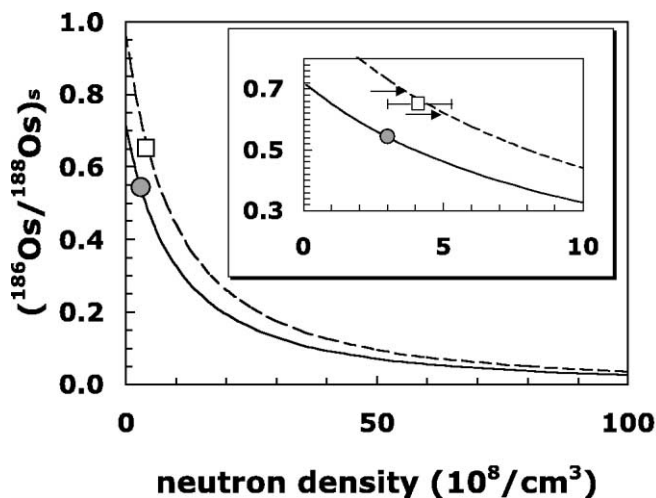


FIG. 3.—The *s*-process  $^{186}\text{Os}/^{188}\text{Os}$  ratio as a function of neutron density with the recommended MACSs (Bao et al. 2000; *dashed curve*) and with the new MACSs (Mosconi et al. 2006; *solid curve*). Also shown are the results of *s*-process  $^{186}\text{Os}/^{188}\text{Os}$  yields and the calculated average *s*-process neutron density in Käppeler et al. (1991; *open square*) and in this study (*gray circle*). The inset features an expanded scale around the estimated average neutron density. Arrows represent *s*-process  $^{186}\text{Os}/^{188}\text{Os}$  yields (Arlandini et al. 1999): *upper arrow*, classical model; *lower arrow*, stellar model.

sical approach are shown on the Bao et al. (2000) MACS curve (Fig. 3). Application of a stellar model with the new MACSs is needed to better estimate the neutron density in the W-Re-Os region.

### 3. DISCUSSION AND SUMMARY

The new isotope anomalies being reported from primitive chondrites (e.g., Brandon et al. 2005; Ranen & Jacobsen 2006; Yokoyama et al. 2007) for heavy elements place stringent demands on  $\sigma_n$  values for use in *s*-process studies. The importance of the present work is in showing that geochemical measurements of isotope anomalies can provide reliable constraints on the ratios of  $\sigma_n$  values (the parameter more relevant to chondrite isotope anomalies than the absolute  $\sigma_n$  values) for any pair of nuclides where no branching occurs in the *s*-process flow. New and precise measurements of the  $\sigma_n$  values are then required mostly for those nuclides that take part in the *s*-process branches.

There is no single neutron density that characterizes the entire *s*-process. The stellar models of Arlandini et al. (1999) show that the neutron densities range from  $10^7$  to  $10^{10}$   $\text{cm}^{-3}$  during *s*-process nucleosynthesis. At the low end of this range, i.e., the asymptotic giant branch (AGB) star interpulse phase, the *s*-process essentially flows through  $^{185}\text{W}$ - $^{185}\text{Re}$ - $^{186}\text{Re}$ - $^{186}\text{Os}$  with no bypassing of  $^{186}\text{Os}$ , and the resulting  $^{186}\text{Os}/^{188}\text{Os}$  ratio (0.71) approximately equals the inverse ratio of their cross sections. (The impact of the new  $\sigma_n$  values can be observed in Fig. 3 since the recommended values of Bao et al. 2000 give this ratio as 0.95.) But during AGB thermal pulses (23 keV), when marginal activation of the  $^{22}\text{Ne}(\alpha, n)^{25}\text{Mg}$  source produces neutron density  $\sim 10^{10}$   $\text{cm}^{-3}$  (see Lugaro et al. 2003 for a detailed discussion), the *s*-process flow largely bypasses  $^{186}\text{Os}$ , yielding  $^{186}\text{Os}/^{188}\text{Os} \sim 0.03$  (Fig. 3). Lugaro et al. (2003) observed that isotope compositions of Sr, Zr, Mo, and Ba in presolar grains were consistent with a marginal activation of the  $^{22}\text{Ne}(\alpha, n)^{25}\text{Mg}$  source during *s*-process nucleosynthesis in solar-metallicity AGB stars. It can be seen that the chondrite *s*-process  $^{186}\text{Os}/^{188}\text{Os}$  anomalies (Fig. 3) are also consistent with this interpretation.

The currently available Os isotope anomaly data (Brandon

et al. 2005; Reisberg et al 2007; Yokoyama et al. 2007) are consistent with a relatively homogenous mixture of *s*-process neutron densities for all aggregate presolar Os carriers. This is particularly evident when comparing bulk chondrite anomalies (Brandon et al. 2005) with Os extracted by thermal combustion from acid-resistant aggregates of presolar grains (Yokoyama et al. 2007). However, the prospect remains that among the acid-resistant mineral phases that host isotopically anomalous Os, new anomalies may be found that sampled nucleosynthetic environments in which the freezeout of the *s*-process occurred at different neutron densities than the solar system average *s*-process. Thus, Os will remain the target of future isotope studies. A particular emphasis is needed for Os isotope measurements on individual presolar grains.

In summary, the ratio of  $\sigma_n$  values in the *s*-process can be determined for any pair of nuclide abundances that have substantial *s*-process contribution from observed isotope anomalies provided that there are no intervening branches along the *s*-process pathway. In this study, we obtained  $\sigma_n(^{190}\text{Os})/\sigma_n(^{188}\text{Os}) = 0.859 \pm 0.042$ , in agreement with previous experimental determinations (0.71–0.84) and with comparable precision ( $\pm 5\%$ ). This result requires that a lower value of  $\sigma_n(^{190}\text{Os}) = 249 \pm 18$  mbarns than the currently recommended value (Bao et al. 2000) should be used with the new  $\sigma_n(^{188}\text{Os})$  (Mosconi et al. 2006), and this result also provides impetus for future measurements of the  $\sigma_n$  values for all Os isotopes. The revised Os  $\sigma_n$  values were then used to obtain the average neutron density in the stellar sites of the solar system *s*-process,  $n_n \sim 3 \times 10^8$   $\text{cm}^{-3}$ , employing the classical approach. The low neutron density obtained for the solar system *s*-process  $^{186}\text{Os}/^{188}\text{Os}$  ratio implies a marginal activation of the  $^{22}\text{Ne}(\alpha, n)^{25}\text{Mg}$  source, consistent with previous results for Sr, Zr, Mo, and Ba isotopes (Lugaro et al. 2003).

We thank the NASA Cosmochemistry Program for its support of this research under NNG06GF50G (M. H.) and RTOP 344-31-72-06 (A. D. B.). We thank Maria Lugaro for her detailed and constructive review that led to substantial improvement of the manuscript.

### REFERENCES

- Allen, B. J., Gibbons, J. H., & Macklin, R. L. 1971, *Adv. Nucl. Phys.*, 4, 205  
 Arlandini, C., Käppeler, F., Wisshak K., Gallino, R., Lugaro, M., Busso, M., & Straniero, O. 1999, *ApJ*, 525, 886  
 Bao, Z. Y., Beer, H., Käppeler, F., Voss, F., & Wisshak, K. 2000, *At. Data Nucl. Data Tables*, 76, 70  
 Brandon, A. D., Humayun, M., Puchtel, I. S., Leya, I., & Zolensky, M. 2005, *Science*, 309, 1233  
 Browne, J., & Berman, B. 1981, *Phys. Rev. C*, 23, 1434  
 Harris, M. J. 1981, *Ap&SS*, 77, 357  
 Holmes, J., Woosley, S. E., Fowler, W., & Zimmerman, B. 1976, *At. Data Nucl. Data Tables*, 18, 305  
 Käppeler, F., Jaag, S., Bao, Z. Y., & Reffo, G. 1991, *ApJ*, 366, 605  
 Lugaro, M., Davis, A. M., Gallino, R., Pellin, M. J., Straniero, O., & Käppeler, F. 2003, *ApJ*, 593, 486  
 Mosconi, M., et al. 2006, in *Nuclei in the Cosmos IX: Ninth Int. Symp. on Nuclear Astrophysics*, 7  
 Nicolussi, G. K., Pellin, M. J., Lewis, R. S., Davis, A. M., Clayton, R. N., & Amari, S. 1998, *ApJ*, 504, 492  
 Papanastassiou, D. A., Chen, J. H., & Wasserburg, G. J. 2004, *Lunar Planet. Sci. Conf.*, 35, 1828  
 Ranen, M. C., & Jacobsen, S. B. 2006, *Science*, 314, 809  
 Rauscher, T., & Thielmann, F.-K. 2000, *At. Data Nucl. Data Tables*, 75, 1  
 Reisberg, L. C., Dauphas, N., Luguet, A., Pearson, D. G., & Gallino, R. 2007, *Lunar Planet. Sci. Conf.*, 38, 1177  
 Sonnabend, K., et al. 2003, *ApJ*, 583, 506  
 Takahashi, K., & Yokoi, K. 1987, *At. Data Nucl. Data Tables*, 36, 375  
 Winters, R., Macklin, R., & Halperin, J. 1980, *Phys. Rev. C*, 21, 563  
 Yin, Q., Jacobsen, S. B., & Yamashita, K. 2002, *Nature*, 415, 881  
 Yokoyama, T., Rai, V. K., Alexander, C. M. O'D., Lewis, R. S., Carlson, R. W., Shirey, S. B., Thiemens, M. H., & Walker, R. J. 2007, *Lunar Planet. Sci. Conf.*, 38, 1151